 CMES, vol.63, no.3, pp.223-242, 2010

Lattice Boltzmann Flow Models for Micro/Nano Fluidics

Kazuhiko Suga[1,2] **and Takahiko Ito**[1]

Abstract: Flow passages in micro/nano-electro-mechanical systems (MEMS/-NEMS) usually have complicated geometries. The present study thus discusses on the latest lattice Boltzmann methods (LBMs) for micro/nano fluidics to evaluate their applicability to micro/nano-flows in complex geometries. Since the flow regime is the continuum to the slip and transitional regime with a moderate Knudsen number (Kn), the LBMs presently focused on feature the wall boundary treatment and the relaxation-time for modeling such flow regimes. The discussed micro flow (μ-flow) LBMs are based on the Bhatnagar-Gross-Krook (BGK) model and the multiple relaxation-time (MRT) model. The presently chosen μ-flow BGK LBM (BGK-1 model) consists of the diffuse-scattering wall condition with the single relaxation–time sensitized to the Knudsen number whereas the μ-flow MRT LBMs are combined with the diffusive bounce-back wall condition (MRT-1 model) and the bounce-back and specular-reflection condition (MRT-2 model). The simulated flow cases are canonical force-driven Poiseuille flows at $0.01 \leq \mathrm{Kn} \leq 10$ and a flow around an obstacle (a square cylinder) situated in a nanochannel at Kn$\approx$0.1. The second-order truncated system (nine discrete velocity model for two dimensions: D2Q9 model) is applied for the simulations. The results show that the MRT models improve the performance of the BGK-1 model. It is also confirmed that the MRT-1 model is superior to the MRT-2 model for simulating micro/nano-flows with impinging and stagnating regions though further improvement is required, particularly, for predicting flow rates.

Keywords: lattice Boltzmann method, Knudsen number, Poiseuille flow, obstacle flow.

[1] Department of Mechanical Engineering, Osaka Prefecture University, Sakai, Osaka 599-8531, Japan

[2] Corresponding author: suga@me.osakafu-u.ac.jp

1 Introduction

Recently, the lattice Boltzmann method (LBM) [McNamara and Zanetti (1988); Higuera and Jimenez (1989)] has been successfully applied in simulating complex flow phenomena [Yu, Luo and Girimaji (2006); Chen, Chang, and Sun (2007); Han, Feng and Owen (2007); Ho, Chan, Lin and Lin (2009); Niu, Hyodo, Suga and Yamaguchi (2009)] including flows in porous media [Keehm, Mukerji and Nur (2004); Pan, Luo and Miller (2006); Suga, Tanaka, Nishio and Murata (2009); Suga and Nishio (2009)] and multiphase flows [Niu, Munekata, Hyodo and Suga (2007); Hao and Cheng (2010)] since it is relatively easy to handle complex flow geometries by the LBM. It should be, however, noted that applying the LBM to micro-flows such as those in micro/nano-electro-mechanical systems (MEMS/NEMS) requires further considerations for the flow physics inside the micro/nano-systems. The flow geometry in those systems is often in a sub-micron meter scale and the flows are usually distinguished by moderate Knudsen numbers: Kn=$\lambda/H > 10^{-2}$, where λ is the molecular mean free path of the fluid and H is the characteristic length of the flow domain. Consequently, the continuum Navier-Stokes equations are no longer applicable to flows at such levels of the Knudsen numbers. The flow physics should be thus described by the Boltzmann equation (BE) of the gas kinetic theory [Chapman and Cowling (1970); Cercignani (1975); Karniadakis, Beskok and Aluru (2005)]. Hence, the direct simulation Monte Carlo (DSMC) simulation has been applied for such MEMS flows, e.g. [Liou and Fang (2000)]. Although the standard LBM was developed for the continuum Navier-Stokes flows, because of its kinetic origin, the LBM has been proven as a basis of schemes to treat micro-flows as well. Indeed, many studies to develop an LBM for micro flows (μ-flow LBM, hereafter) have been made so far.

In order to treat flows at moderate Kn, Nie et al. [Nie, Doolen and Chen (2002)] introduced Kn dependency into the relaxation parameter of the lattice Boltzmann equation and simulated two-dimensional (2-D) microchannel and cavity flows at 0.01<Kn<0.4 with the conventional bounce-back wall boundary condition. Shen et al. [Shen, Tian, Xie and Fan (2004)] validated this strategy comparing with the DSMC simulations of microchannel flows. Succi [Succi (2002)] introduced a combination of bounce-back and specular reflections for the wall boundary condition. Referring to the analytical velocity slip condition, Sbragaglia and Succi [Sbragaglia and Succi (2005)] discussed this slip-reflection model as well as the slip-reflection-accommodation model in which the accommodation effect on the walls is introduced. They showed that the models could be tuned to recover quantitative agreement with the analytical and experimental results. Toschi and Succi [Toschi and Succi (2005)] introduced a virtual wall collision concept into the bounce-back and diffuse-scattering boundary conditions of Ansumali and Karlin [Ansumali and Kar-

lin (2002)]. Zhang et al. [Zhang, Qin, and Emerson (2005)] applied a Maxwellian scattering kernel to the wall conditions with an accommodation coefficient. Guo and Zheng [Guo and Zheng (2009)] summarized wall boundary treatments and showed that the bounce-back/specular-reflection, the diffuse-scattering and the diffusive bounce-back models could be converted to a mathematically equivalent form for prescribing the slip velocity on the wall.

As for the relaxation time, to address the Knudsen layer effect, Zhang et al. [Zhang, Gu, Barber and Emerson (2006)] and Guo et al. [Guo, Zhao, Shi (2006)] modified the relaxation time by an effective mean free path. Although most of the above LBM studies were based on the single relaxation-time (SRT) Bhatnagar-Gross-Krook (BGK) model [Bhatnagar, Gross and Krook (1954)], Guo et al. [Guo, Zheng and Shi (2008)] discussed the multiple relaxation-time (MRT) method [d'Humieres, Ginzburg, Krafczyk, Lallemand and Luo (2002)] with the combination of the bounce-back and the specular reflection wall boundary condition of Succi. Verhaeghe et al. [Verhaeghe, Luo and Blanpain (2009)] proposed a diffusive bounce-back model that is the combination of the diffuse-scattering and bounce-back boundary conditions for fully diffusive stationary walls in the context of the MRT LBM.

As aforementioned, many LBM studies have been devoted to simulate micro-flows. However, almost all proposals in the literature have been validated only in simple canonical flows such as the Couette and Poiseuille flows. Hence, it is now important to provide information indicating whether those schemes perform well or not in more complex impinging and stagnating flows. Therefore, recently the present authors' group attempted to validate an LBM in a flow around a square cylinder situated in a nanochannel [Suga, Takenaka, Ito, Kaneda, Kinjo and Hyodo (2010)]. Their validated LBM [Niu, Hyodo, Munekata and Suga (2007)] was based on the diffuse-scattering boundary condition and the SRT BGK model sensitized to Kn with the regularization procedure of the nonequilibrium part of the distribution function [Zhang, Shang and Chen (2006)]. (This BGK LBM is called the BGK-1 model, hereafter.) They also performed the molecular dynamics (MD) simulation using the Lennard-Jones potential [Koplik and Banavar (1995); Haile (1997)] to produce the reference data. In their report, since the square cylinder flow results by the LBM and the MD simulations were in good agreement, they concluded that the BGK-1 model was applicable to complex micro/nano-flows. Moreover, although the BGK-1 model with the conventional two-dimensional nine discrete velocity (D2Q9) model predicted flow fields less accurately in the canonical Poiseuille and Couette flows, its predictive accuracy became comparable to that with the two-dimensional twenty-one discrete velocity (D2Q21) model when applied to the square cylinder flow.

However, in many flow cases including flows in complex geometries, it is now

recognized that the MRT model is generally more stable and superior to the BGK model. Pan et al. [Pan, Luo and Miller (2006)] reported that it overcame the defect of the BGK model which is the viscosity dependency of flows when solid boundary is present, particularly in complex porous medium flows. Since our final goal is to establish a cost-effective stable scheme to simulate complex micro/nano-flows, the MRT based μ-flow LBMs should be discussed. Therefore, the present study compares the performance of our previously evaluated BGK-1 model and the MRT μ-flow LBMs of Verhaeghe et al. [Verhaeghe, Luo and Blanpain (2009)] (named the MRT-1 model), and of Guo et al. [Guo, Zheng and Shi (2008)] (named the MRT-2 model). The MRT-1 model applies the diffusive bounce-back boundary model which is a modified model of the diffuse-scattering boundary model used in the BGK-1 model whilst the MRT-2 model applies the combination of the bounce-back and specular reflection boundary model. The present MRT-1 and MRT-2 models are slightly modified from the original forms as described in Section 2.2. The chosen test flow cases are the canonical force driven Poiseuille flows and the square cylinder flow of Suga et al. [Suga, Takenaka, Ito, Kaneda, Kinjo and Hyodo (2010)].

2 Numerical Schemes of the μ-flow Lattice Boltzmann Method

Although one should refer to the original papers [Niu, Hyodo, Munekata and Suga (2007); Verhaeghe, Luo and Blanpain (2009); Guo, Zheng and Shi (2008)] for the detailed derivation of the lattice Boltzmann equations (LBEs) and their modeling steps for applying to micro/nano-flows, their brief descriptions are given below.

2.1 BGK μ-flow LBM (BGK-1)

The LBE can be obtained by discretizing the velocity space of the BE into a finite number of discrete velocities $\xi_\alpha \{\alpha = 0, 1, \cdots, Q-1\}$. Although many techniques to discretize the velocity space have been proposed, in the present study, the BGK μ-flow LBM: BGK-1 model, employs the D2Q9 model for 2-D flows. Note that the original BGK-1 model was coupled with the D2Q21 model. However, Suga et al. [Suga, Takenaka, Ito, Kaneda, Kinjo and Hyodo (2010)] reported that the BGK-1 model with the D2Q9 performed comparable to that with the D2Q21 model in a relatively complex flow case: the square cylinder flow. Table 1 lists the sound speed c_s, the discrete velocity ξ_α and the weight parameter ω_α in the D2Q9 model. Let $\mathbf{x}$ be the Cartesian coordinates of the configuration space and ξ that of the velocity space. The LBE describes evolutions of a single particle distribution function $f(\mathbf{x}, \xi, t)$ defined such that $f(\mathbf{x}, \xi, t) d\xi d\mathbf{x}$ represents the number of particles in the

phase space element $d\xi d\mathbf{x}$ time t, and can be written in the following BGK form:

$$f_\alpha(\mathbf{x}+\xi_\alpha\delta t, t+\delta t) = f_\alpha(\mathbf{x},t) - \frac{\delta t}{\tau+0.5\delta t}\left(f_\alpha(\mathbf{x},t) - f_\alpha^{eq}(\mathbf{x},t)\right) + \frac{\tau\delta t}{\tau+0.5\delta t}F_\alpha(\mathbf{x},t) \quad (1)$$

where the equilibrium distribution function f^{eq} is written as

$$f_\alpha^{eq}(\mathbf{x},t) = \omega_\alpha\rho\left\{1+\frac{\xi_\alpha\cdot\mathbf{u}}{RT}+\frac{1}{2}\left[\frac{(\xi_\alpha\cdot\mathbf{u})^2}{(RT)^2}-\frac{\mathbf{u}^2}{RT}\right]\right\}. \quad (2)$$

Equation (2) retains up to the second-order term in the Hermite expansion. The ideal gas constant is R, and ρ, $\mathbf{u}$ and T are respectively the fluid macro density, velocity and temperature. The sound speed $c_s = \sqrt{RT}$ is equal to $\sqrt{1/3}$ in the D2Q9 model. The contribution of the force term F_α is introduced as

$$F_\alpha(\mathbf{x},t) = \omega_\alpha\rho\left\{\left[\frac{\xi_\alpha\cdot\mathbf{a}}{RT}\left(1+\frac{\xi_\alpha\cdot\mathbf{u}}{RT}\right)-\frac{\mathbf{a}\cdot\mathbf{u}}{RT}\right]\right\}, \quad (3)$$

where $\mathbf{a}$ is the acceleration of the force. The variables ρ, $\mathbf{u}$ and the pressure p are respectively obtained by applying the integral of microscopic velocity moment as

$$\rho = \sum_{\alpha=0}^{Q-1} f_\alpha, \quad \rho\mathbf{u} = \sum_{\alpha=0}^{Q-1} f_\alpha\xi_\alpha + \frac{\delta t}{2}\mathbf{a}, \quad p = \rho c_s^2. \quad (4)$$

So far, the equations which govern the macroscopic variables of continuum flows are presented. Only when the non-equilibrium part of distribution is very small and the distribution function can be approximated by the equilibrium distribution function, the equations can describe the fluid phenomena. However, when the Kn becomes larger and the non-equilibrium part is no longer ignorable, the aforementioned LBE becomes invalid. According to our previous analysis, the difficulty is cleared by using the three procedures briefly described below. (See [Niu, Hyodo, Munekata and Suga (2007)] for more details.)

Table 1: Main parameters of the D2Q9 model for the 2-D BGK LBM.

model	c_s^2	ξ_α	ω_α
D2Q9	1/3	(0,0)	4/9($\alpha=0$)
		$(\pm1,0)$, $(0,\pm1)$	1/9(α=1-4)
		$(\pm1,\pm1)$	1/36(α =5-8)

2.1.1 Diffuse-scattering boundary condition

The non-slip wall boundary conditions used in the continuum LBM are based on perfect reflection, so the velocity and the temperature of a wall are not reflected into the distribution of the reflected particles. However, from a microscopic viewpoint, the wall boundary condition should include the physics on the wall because the fluid and the wall molecules are interacted with each other. Therefore, the incident particles are modeled to be reflected with the information of the Maxwell distribution function at the wall boundary. The modeled form is written in the LBM frame as

$$f_\alpha(\mathbf{x},t) = \frac{\sum_{\alpha'} |(\xi'_\alpha - \mathbf{u}_w)\cdot\mathbf{n}| f_{\alpha'}(\mathbf{x},t)}{\sum_{\alpha'} |(\xi'_\alpha - \mathbf{u}_w)\cdot\mathbf{n}| f^{eq}_{\alpha'}(\mathbf{x},t)} f^{eq}_{\alpha,w}(\mathbf{x},t) := f^D_\alpha(\mathbf{x},t),$$

if

$$\left[(\xi'_\alpha - \mathbf{u}_w)\cdot\mathbf{n} < 0;\ (\xi_\alpha - \mathbf{u}_w)\cdot\mathbf{n} > 0\right], \tag{5}$$

where $\mathbf{n}$ is the unit wall normal vector, ξ'_α is the velocity of incident particles, $f^{eq}_{\alpha,w}$ is the wall equilibrium distribution function, and the subscripts w, α', α respectively denote the wall and the directions of the incident and reflected particles.

2.1.2 Effective relaxation time

In continuum flow, the relaxation-time τ can be defined in terms of viscosity μ, then flow is under control of the Reynolds number. In contrast, Kn is a fundamental dimensionless number in non-continuum flow. Therefore, for applying to moderate Kn flows, the relaxation-time needs to be associated with Kn. In microscale wall bounded geometries, the mean free path of the total molecules in the system should be smaller than that in the unbounded systems due to the wall effects. Stops [Stops (1970)] then introduced a correction function $\Psi(\mathrm{Kn})$ to the molecular mean free path as $\lambda^* = \lambda\Psi$. Since the relaxation-time τ can be expressed as $\tau = \sqrt{2/\pi}\, c_s \lambda$, the effective relaxation-time τ^* can be modeled as

$$\tau^* = \tau\Psi(\mathrm{Kn}), \tag{6}$$

where Kn is still the conventional Knudsen number without considering the wall effects. However, in this study, it is defined using the local density to include local effects as

$$\mathrm{Kn}^* = \frac{\mu}{\rho H}\sqrt{\frac{\pi}{2RT}}. \tag{7}$$

The function Ψ derived by Stops was very complicated and difficult for particular applications, Guo et al. [Guo, Zhao and Shi (2006)] thus approximated Stops' Ψ function by a simple formula as

$$\Psi(x) = \frac{2}{\pi}\arctan(\sqrt{2}x^{-3/4}), \tag{8}$$

where $x = \mathrm{Kn}^*$ in this study. The functional behavior (Ψ decreases as Kn^* increases) indicates that some molecules will hit walls and their flight time (effective relaxation-time τ^*) may be shorter than the mean free time defined in an unbounded system.

2.1.3 Regularization procedure

Generally speaking, the distribution function f_α has an aliasing error because it cannot be entirely projected on to the Hermite space. Such an error is usually very small, but it can be no longer neglected when the system is far from equilibrium because of high Knudsen number effects. To resolve this problem, the regularization procedure was previously introduced for improving numerical stability [Zhang, Shang and Chen (2006)]. The procedure is implemented as the following. First, the distribution function f_α is divided as

$$f_\alpha = f_\alpha^{eq} + f'_\alpha, \tag{9}$$

where f'_α is the non-equilibrium part of the distribution. Second, it is necessary to convert f'_α to a new distribution $\tilde{f}'_\alpha$ which lies within the subspace spanned by the first three Hermite polynomials. Using the Hermite polynomials, $\tilde{f}'_\alpha$ is expressed for the D2Q9 model as

$$\tilde{f}'_\alpha = \omega_\alpha \left[\frac{1}{2c_s^2} H^{(2)}\left(\frac{\xi_\alpha}{c_s}\right) \sum_{\alpha=o}^{Q-1} f'_\alpha \xi_{\alpha i}\xi_{\alpha j} \right], \tag{10}$$

where, $H^{(n)}(x)$ is the nth order Hermite polynomial of a variable x. By replacing f_α in Eq.(1) with Eq.(9) after converting f'_α in Eq.(9) to $\tilde{f}'_\alpha$ in Eq.(10), one can obtain the following form:

$$f_\alpha(\mathbf{x}+\xi_\alpha\delta t, t+\delta t) = f_\alpha^{eq}(\mathbf{x},t) + \frac{\tau - 0.5\delta t}{\tau + 0.5\delta t}\tilde{f}'_\alpha + \frac{\tau\delta t}{\tau+0.5\delta t}F_\alpha(\mathbf{x},t). \tag{11}$$

2.2 MRT μ-flow LBMs

The MRT LBM [d'Humieres, Ginzburg, Krafczyk, Lallemand and Luo (2002)] transforms the distribution function in the velocity space to the moment space by a

transformation matrix. Since the moments of the distribution function correspond directly to flow quantities, the moment representation allows us to perform the relaxation processes with different relaxation-times according to different time-scales of various physical processes. The evolution equation is thus written as

$$\frac{1}{\delta t}\left[|\mathbf{f}(\mathbf{x}+\xi_\alpha\delta t, t+\delta t)\rangle - |\mathbf{f}(\mathbf{x},t)\rangle\right] = -\mathbf{M}^{-1}\widehat{\mathbf{S}}\left[|\mathbf{m}(\mathbf{x},t)\rangle - |\mathbf{m}^{eq}(\mathbf{x},t)\rangle\right] + |\mathbf{F}\rangle, \quad (12)$$

where the bracketed vector such as $|\mathbf{f}\rangle$ means $|\mathbf{f}\rangle := (f_0, f_1, \cdots, f_{Q-1})^T$. The matrix $\mathbf{M}$ is a $Q \times Q$ matrix which linearly transforms the distribution function $\mathbf{f}$ to the velocity moment $\mathbf{m}$:

$$\mathbf{M} = \begin{pmatrix} 1 & 1 & 1 & 1 & 1 & 1 & 1 & 1 & 1 \\ -4 & -1 & -1 & -1 & -1 & 2 & 2 & 2 & 2 \\ 4 & -2 & -2 & -2 & -2 & 1 & 1 & 1 & 1 \\ 0 & 1 & 0 & -1 & 0 & 1 & -1 & -1 & 1 \\ 0 & -2 & 0 & 2 & 0 & 1 & -1 & -1 & 1 \\ 0 & 0 & 1 & 0 & -1 & 1 & 1 & -1 & -1 \\ 0 & 0 & -2 & 0 & 2 & 1 & 1 & -1 & -1 \\ 0 & 1 & -1 & 1 & -1 & 0 & 0 & 0 & 0 \\ 0 & 0 & 0 & 0 & 0 & 1 & -1 & 1 & -1 \end{pmatrix}, \quad (13)$$

for the D2Q9 model and the collision matrix $\widehat{\mathbf{S}} = \mathbf{M}\cdot\mathbf{S}\cdot\mathbf{M}^{-1}$ is diagonal:

$$\widehat{\mathbf{S}} = diag(s_0, s_1, \cdots, s_8). \quad (14)$$

The moment components have physical significances:

$$\mathbf{m} = (\rho, e, \varepsilon, j_x, q_x, j_y, q_y, p_{xx}, p_{xy}), \quad (15)$$

where the density ρ and the momentum $\mathbf{j} := \rho\mathbf{u} = (j_x, j_y)$ are conserved moments. The other six non-conserved moments, e, ε, $\mathbf{q} := (q_x, q_y)$, p_{xx} and p_{xy} are, respectively, related to the energy, the energy square, the heat flux, the diagonal and off-diagonal components of the stress tensor. The equilibria of the conserved moments are themselves and those of the non-conserved moments are

$$e^{eq} = 3\mathbf{j}\cdot\mathbf{j} - 2\rho,\ \varepsilon^{eq} = \rho - 3\mathbf{j}\cdot\mathbf{j},\ q_x^{eq} = -j_x,\ q_y^{eq} = -j_y, \quad p_{xx}^{eq} = j_x^2 - j_y^2,\ p_{xy}^{eq} = j_x j_y. \quad (16)$$

Following Lallemand and Luo [Lallemand and Luo (2000)], the kinetic viscosity $\nu = \mu/\rho$ and the bulk viscosity ζ are given as

$$\nu = c_s^2\left(\frac{1}{s_\nu} - \frac{1}{2}\right)\delta t, \quad (17)$$

$$\zeta = \frac{c_s^2}{2}\left(\frac{1}{s_e} - \frac{1}{2}\right)\delta t, \tag{18}$$

where $s_\nu = s_7 = s_8$ is the relaxation rate for the moments related to the stress and $s_e = s_1$ is the relaxation rate for the moment related to the energy.

2.2.1 The MRT-1 model

The MRT-1 model by Verhaeghe et al. [Verhaeghe, Luo and Blanpain (2009)] applies $s_i = s_\nu$ for $i = 0,1,2,3,5,7,8$ and $s_q = s_4 = s_6$ with

$$s_q = \frac{8(2-s_\nu)}{8-s_\nu}, \tag{19}$$

following Ginzbourg and Adler [Ginzbourg and Adler (1994)]. The relaxation rate s_ν is defined by Eq.(17) with fixed viscosity. However, since the viscosity is written as $\mu = \rho\lambda\sqrt{2c_s^2/\pi}$, with the effective molecular mean free path λ^* discussed in Section 2.1.2, Eq.(17) can be rewritten as

$$s_\nu^{-1} = \frac{1}{2} + \frac{\lambda\Psi}{c_s\delta t}\sqrt{\frac{2}{\pi}} = \frac{1}{2} + \frac{H}{c_s\delta t}\sqrt{\frac{2}{\pi}}\mathrm{Kn}\Psi. \tag{20}$$

For the Ψ function, Eq.(8) is applied. (Indeed, we have found that this modification leads to better performance than that of the original form in predicting the Poiseuille flows.)

The MRT-1 model applies the diffusive bounce-back boundary condition that is the combination of the diffuse-scattering and bounce-back boundary conditions for the wall boundary as

$$f_\alpha(\mathbf{x}, t+\delta t) = b\, f_\beta(\mathbf{x}, t) + (1-b)\, f_\alpha^D(\mathbf{x}, t+\delta t), \tag{21}$$

where b is a probability coefficient taking $b = 0.0 - 1.0$, the bounce-back vectors are $\xi_\beta = -\xi_\alpha$ and f_α^D is the diffuse scattering model given by Eq.(5). This model turns into the diffuse scattering model when $b \Rightarrow 0$, whilst it becomes the (non-slip) bounce-back model with $b = 1$. To satisfy the first-order slip velocity for the microscopic slip velocity, Verhaeghe et al. derived the probability coefficient:

$$b = \frac{3\mu - \mathrm{Kn}H\bar{\rho}_{out}\delta_x/\delta t}{3\mu + \mathrm{Kn}H\bar{\rho}_{out}\delta_x/\delta t}, \tag{22}$$

where δ_x is the lattice spacing. This form can be rewritten as

$$b = \frac{3\rho\sqrt{2c_s^2/\pi} - \bar{\rho}_{out}\delta_x/\delta t}{3\rho\sqrt{2c_s^2/\pi} + \bar{\rho}_{out}\delta_x/\delta t}, \tag{23}$$

which is independent of Kn. In 2-D incompressible flow cases where $\delta_x = \delta t = 1$, the probability is almost constant as $b \approx 0.16$.

2.2.2 The MRT-2 model

The presently applied MRT-2 model of Guo et al. [Guo, Zheng and Shi (2008)] applies $s_0 = s_3 = s_5 = 1$, $s_1 = 1/1.1$, $s_2 = 1/1.2$. (Although they optimized these values, they reported that the relaxation rates except for s_ν and s_q had negligible influence on the simulation results.) Although the relaxation rate s_ν is defined by Eq.(17) with the viscosity, Guo et al. modified it using the effective molecular mean free path $\lambda^*(=\lambda\Psi)$ as shown in Eq.(20). For the Ψ function, although Guo et al. used another function of Kn and the distance from the wall, the present MRT-2 model applies Eq.(8). The relaxation rates_q is given by

$$\widetilde{\tau}_q = \frac{3+24\chi^2\left(\widetilde{\tau}_s(0)\right)^2 A_2}{16\widetilde{\tau}_s(0)} + \frac{\tau_s'(0)\delta_x[12+30\widetilde{\tau}_s(0)\chi A_1]}{16\left(\widetilde{\tau}_s(0)\right)^2}, \tag{24}$$

where $\widetilde{\tau}_q = 1/s_q - 0.5$, $\tau_s = 1/s_\nu$, $\widetilde{\tau}_s = \tau_s - 0.5$,$\tau_s(0) = \tau_s|_{wall}$, $\tau_s'(0) = \partial\tau_s/\partial n|_{wall}$ and n is the wall-normal direction. The coefficients are $\chi = \sqrt{\pi/6}$, $A_1 = \frac{2-\sigma_a}{\sigma_a}(1 - 0.1817\sigma_a)$ and $A_2 = 1/\pi + A_1^2/2$ where σ_a is the accommodation coefficient. (In all the present test flow cases where the walls are diffusive, $\sigma_a = 1$ is applied.) This relaxation-time was derived by discussing a second-order slip boundary condition for the microscopic slip velocity when the combined bounce-back and specular-reflection model was used. It is, however, obviously difficult to apply Eq.(24) to complex surface geometry. Indeed, nobody can answer which $\tau_s(0)$ is used for the region away from the walls such as the core region of a rectangular sectioned duct since the original S_ν, and thus Z_s include dependency on the distance from the wall. Therefore, although it may damage the original performance, the MRT-2 model in this study simply truncates the model as

$$\widetilde{\tau}_q = \frac{3+24\chi^2\widetilde{\tau}_s^2 A_2}{16\widetilde{\tau}_s}. \tag{25}$$

The MRT-2 model employs the combined bounce-back and specular-reflection boundary condition for slippage at a solid wall in a micro flow originally proposed by Succi [Succi (2002)]. In this scheme, it is assumed that some of the particles hitting a solid wall bounce back but the others reflect specularly. It is expressed as

$$f_\alpha(\mathbf{x}, t+\delta t) = r_s\, f_\beta(\mathbf{x}, t) + (1-r_s)\, f_\gamma(\mathbf{x}, t), \tag{26}$$

where r_s is a bridge coefficient taking $r_s = 0.0 - 1.0$ and vectors $\xi_\beta = -\xi_\alpha$ and $\xi_\gamma = \xi_\alpha - 2(\xi_\alpha \cdot \mathbf{n})\mathbf{n}$ are, respectively, the inverse and the specular symmetric velocity vectors of ξ_α. By discussing the second-order slip boundary condition for

the microscopic slip velocity, Guo et al. [Guo, Zheng and Shi (2008)] derived the bridge coefficient as

$$r_s = \left[1 + \chi A_1 + \frac{\tau_s'(0)\delta_x}{8(\widetilde{\tau}_s(0))^2}\right]^{-1}, \tag{27}$$

which is again difficult to apply to complex surface geometry. Thus, the present MRT-2 model truncates it as

$$r_s = [1 + \chi A_1]^{-1}, \tag{28}$$

which becomes $r_s = 0.628$ in the present study.

3 Results and Discussions

Simulations of canonical flows are firstly discussed and then, a flow around a square cylinder in a nanochannel [Suga, Takenaka, Ito, Kaneda, Kinjo and Hyodo (2010)] is discussed.

3.1 3.1 Force driven Poiseuille flows

Figure 1 compares the velocity profiles of plane Poiseuille channel flows at Kn = 0.01 to 10 with the data of the DSMC by Beskok and Karniadakis [Beskok and Karniadakis (1999)] with fully diffusive wall boundary conditions (the accommodation coefficient is 1.0). These velocity profiles are normalized by the mean velocity U_b and the wall normal distance y is normalized by the channel height H. The 2-D uniform Cartesian lattice of 100×100 is used for the simulations. (This density of the lattice was confirmed to be more than fine enough by our previous study [Niu, Hyodo, Munekata and Suga (2007)]). The number of iterations of the LBM simulations is 5,000 and the results are fully converged.

As in our previous studies [Niu, Hyodo, Munekata and Suga (2007); Suga, Takenaka, Ito, Kaneda, Kinjo and Hyodo (2010)], although the BGK-1 model with the D2Q21 model well captures Knudsen number effects in the Poiseuille flows, the BGK-1 model with the D2Q9 model is not very accurate. Yet, even with the less accurate D2Q9 model, as shown in Fig.1, the BGK-1 model can capture the general flow tendency, though its results always show a little deviation from those of the DSMC up to Kn=1. The MRT models, however, perform better than the BGK-1 model up to Kn=1. This is because in both the MRT-1 and MRT-2 models, the boundary conditions were optimized by discussing the first or the second-order slip boundary condition for the microscopic slip velocity.

However, as shown in Fig.1(d) at Kn=10, the BGK-1 model agrees better with the DSMC. This leads to the better agreement with the DSMC and the linearized BE

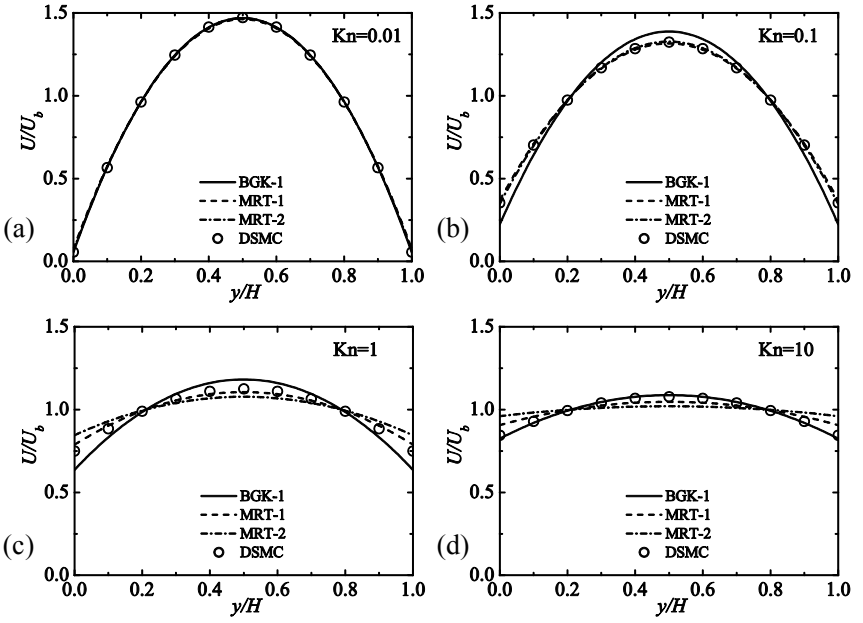

Figure 1: Velocity profile comparisons of the μ-flow LBMs in Poiseuille flows; (a) at Kn=0.01, (b) at Kn=0.1, (c) at Kn=1.0, and (d) at Kn=10; the DSMC data are from [Beskok and Karniadakis (1999)].

in the slip and centerline velocities: U_s, U_c, at Kn>2 as shown in Fig.2(a). It is however clear that both the MRT models predict the slip velocity very accurately at Kn<0.2. As for the centerline velocity U_c, the MRT models always predict satisfactory results. As shown in Fig.2(b), the mass flow rate:

$$Q = \sum_{y=0}^{H} \rho U(y)/(\rho \mathbf{a}_x H^2/c_s), \tag{29}$$

is satisfactorily predicted only by the MRT-2 model at $0.01 \leq \mathrm{Kn} \leq 10$. This suggests that the MRT-1 model needs further optimization by considering the higher order slip velocity condition as made in the MRT-2 model. This is because the near-wall velocity profile affects the slip velocity and the wall shear stress which significantly correlates with the flow rate. Note that the BGK-1 model predicts the flow rare satisfactorily when the D2Q21 model is coupled [Niu, Hyodo, Munekata and Suga (2007)]. It is thus clear that applying the higher order discrete velocity model gives improvement of the prediction accuracy. Yet, since boundary treat-

ments become too complicated in complex geometries, it is better to avoid applying such higher order discrete velocity models if possible.

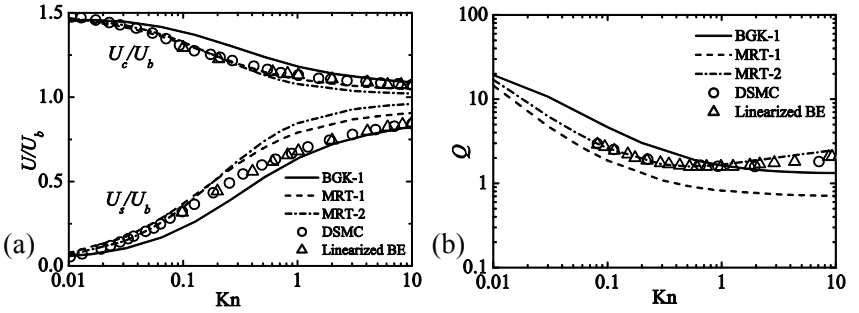

Figure 2: Dependency of the flow characteristics on Kn; (a) velocity scaling at wall and centerline of the channels, and (b) flow rate; the DSMC data are from Karniadakis, Beskok and Aluru (2005), the linearized BE data are from [Ohwada, Sone and Aoki (1989)].

3.2 Square cylinder flow

A square cylinder flow: a flow around a square cylinder placed in a nanochannel, is considered. Figure 3(a) illustrates the flow geometry in which a square cylinder whose section is $H/5 \times H/5$ is located at the center of a nanochannel. Periodic boundary conditions are applied to the inlet and outlet boundary and thus, the flow regime is regarded as a part of an infinite cylinder array set in a nanochannel. The force is applied to the x-direction only and the Knudsen number is Kn=0.084 as in the MD simulation of Suga, Takenaka, Ito, Kaneda, Kinjo and Hyodo (2010). In their MD simulation, the channel height and the square cylinder width were set as respectively 28σ and 5.6σ, where σ is the diameter of the molecules (they correspond to 9.5 and 1.9 nm, respectively). The computational domain applied was $28\sigma \times 28\sigma \times 27.886\sigma$ and 6642 fluid molecules surrounded by 4738 wall molecules of argon monolayers were simulated. Although the flow geometry of the MD simulation was three dimensional, the 2-D statistic flow characteristics were obtained by averaging in the spanwise direction.

Thus, all the LBM simulations are carried out on the 2-D grid whose size is 100×100. (After a series of grid dependency tests using grids of 50×50 to 200×200, results by the grid of 100×100 are confirmed to be grid independent.) The number of iterations of the LBM simulations is around 40,000 and the results are fully

converged. Figure 3(b) shows streamlines obtained by the simulation. The flow impinges onto the square cylinder forming stagnation points on the upstream and downstream faces.

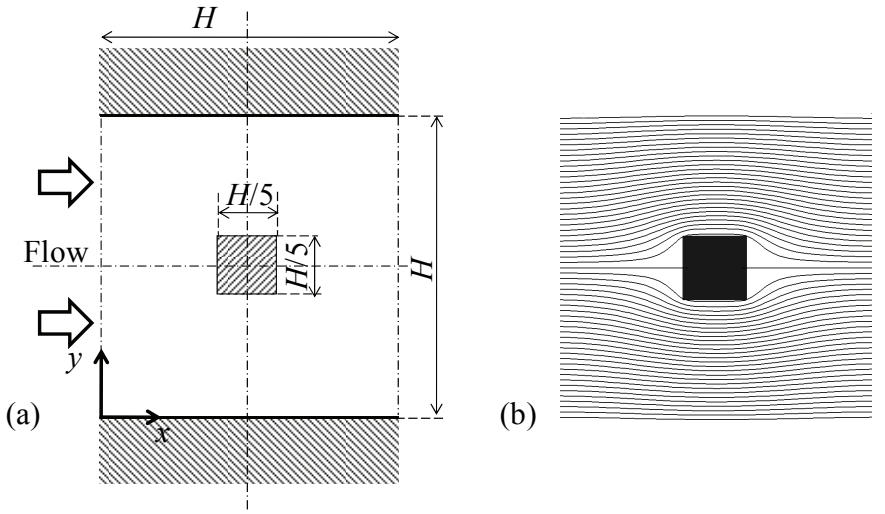

Figure 3: Flow around a square cylinder in a nanochannel; (a) schematic view, and (b) streamlines.

Figure 4 compares the normalized streamwise velocity U profiles by the bulk mean velocity U_b at $x/H = 0.0$, 0.25, 0.5 and 0.75. These distribution profiles of the LBM simulations generally agree with those of the MD simulation with difference of up to 5 percent of the bulk mean velocity. At $x/H = 0.0$, compared with the BGK-1 model, both the MRT models show better agreement with the MD simulation, particularly near the walls and in the center region. This is partly because the MRT model can predict the slippage velocity better at the wall at Kn$\approx$ 0.1 as shown in Fig.2(a). (Figure 2(a) indicates that both the MRT models accurately predict the slippage velocity U_s whilst the BGK-1 model underpredicts U_s at Kn$\leq$ 0.1.) As seen in the center region of Fig.4(a), the BGK-1 model predicts the velocity recovery faster than those of the MRT models and the MD. This confirms that it is the SRT model that leads to too rapid flow development or recovery from velocity defect in the wake behind the obstacle. However, as shown in Figs.4(c) and (d), the predictive accuracy of the MRT-2 model becomes slightly lower than those of the BGK-1 and MRT-1 models at x/H=0.5 and 0.75.

The difference in the wall boundary conditions clearly seen in Fig.5 which com-

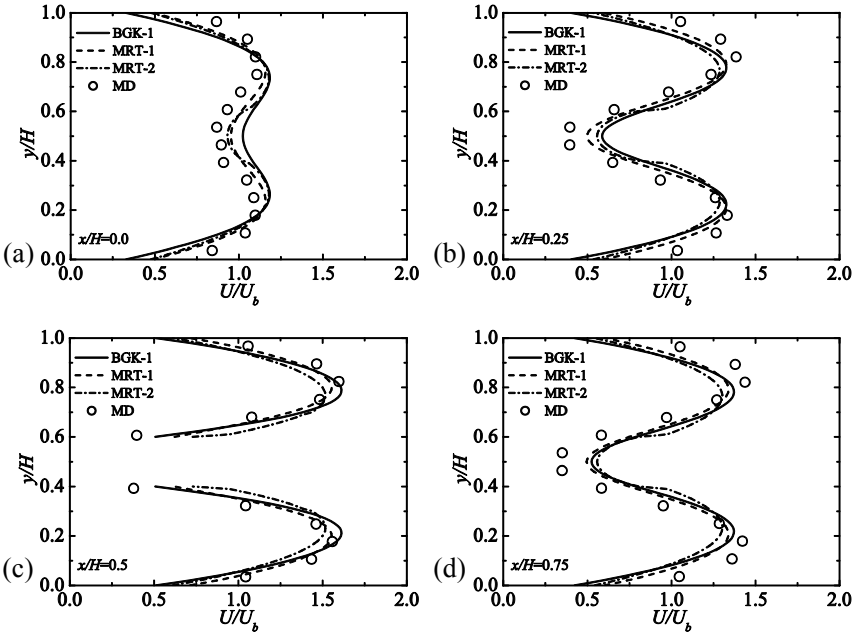

Figure 4: Comparison of streamwise velocity around a square cylinder in a nanochannel at Kn=0.084; (a) at $x/H = 0.0$, (b) at $x/H = 0.25$, (c) at $x/H = 0.5$, (d) at $x/H = 0.75$.

pares wall normal velocity V profiles at x/H =0.25, 0.4, 0.6 and 0.75. The regions of $0.4 \leq y/H \leq 0.6$ at $x/H = 0.4$ (Fig.5(b)) and 0.6 (Fig.5(c)) respectively correspond to the foreface and back-face of the square cylinder. As shown in Fig.3(b), the flow impinges onto the foreface and then slides along it. On the back-face, the flow slides along the face to the stagnation point. These flow motions are well predicted by the MRT-1 model as indicated in Fig.5(b)) and (c). Obviously, at the corners: y/H=0.4 and 0.6, only the MRT-1 model captures well the peak levels of the velocity profiles whereas the other models overpredict them and the slippage velocities by more than 10 percent of U_b. At the sections of x/H =0.25 and 0.75, Figs.5(a) and (d) indicate that the MRT-2 model performs slightly worse than the other μ-flow LBMs. The above comparisons confirm that the combination of the bounce-back model with the diffuse-scattering condition improves the performance of the diffuse-scattering boundary condition and superior to the combined bounce-back and specular-reflection boundary condition.

Note that in the BGK-1 model, the regularization procedure is required since with-

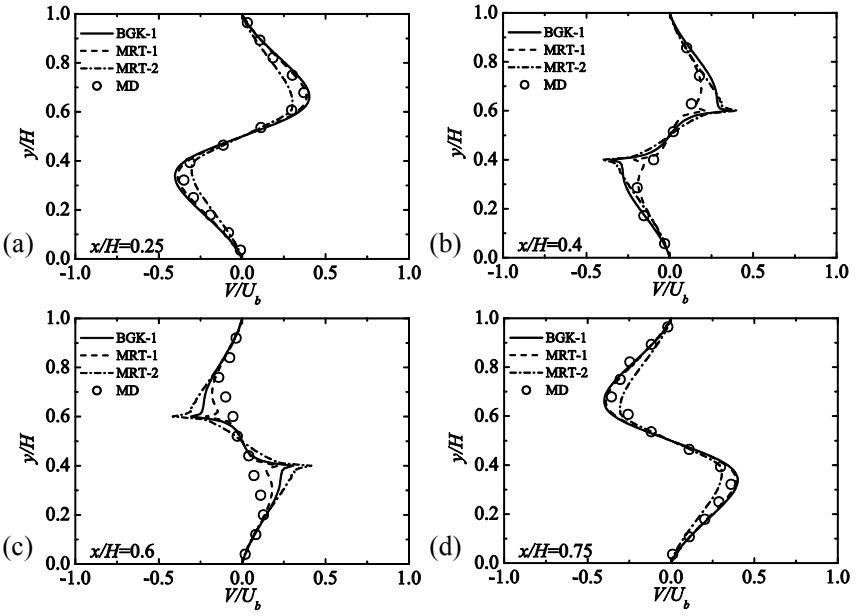

Figure 5: Comparison of wall-normal velocity around a square cylinder in a nanochannel at Kn=0.084; (a) at $x/H = 0.25$, (b) at $x/H = 0.4$, (c) at $x/H = 0.6$, and (d) at $x/H = 0.75$.

out it the BGK based models express oscillative velocity profiles as also discussed in [Suga, Takenaka, Ito, Kaneda, Kinjo and Hyodo (2010); Suga, Takenaka, Ito and Kaneda (2010)]. By the MRT models, however, such a process is not needed to damp the oscillations. This also proves that the MRT models are more stable for micro/nano-flow applications at this level of Kn.

4 Conclusions

In this study, flow simulations at moderate Knudsen numbers are performed by both the SRT BGK (BGK-1 model) and the MRT based μ-flow LBMs (MRT-1, MRT-2 models). The BGK-1 model consists of the diffuse-scattering boundary condition and the single relaxation-time sensitized to Kn with the regularization procedure of the nonequilibrium part of the distribution function. The MRT-1 model consists of the diffusive bounce-back boundary model that is the combination of the diffuse-scattering and bounce-back boundary conditions whilst the MRT-2 model consists of the combined bounce-back and specular-reflection boundary condition

for slippage at a solid wall. The D2Q9 model is applied to all the cases. The simulated flow cases are canonical force-driven Poiseuille flows at $0.01 \leq \mathrm{Kn} \leq 10$ and a flow around a square cylinder situated in a nanochannel at Kn=0.084. It is confirmed that although all the tested μ-flow LBMs successfully reproduce characteristic velocity profiles of the Poiseuille flows at moderate Knudsen numbers, the MRT models perform better than the BGK model. Among the evaluated MRT models, the MRT-2 model predicts better the flow rates than the MRT-1 model. This suggests that further improvement for the MRT-1 model is required by considering the higher order slip boundary condition as made in the MRT-2 model. In the square cylinder flow, the MRT models improve the BGK model's rapid flow recovery in the wake behind the square cylinder. It is also confirmed that the combination of the bounce-back model with the diffuse scattering condition improves the performance of the diffuse-scattering boundary condition and it is superior to the combined bounce-back and specular-reflection boundary condition around the stagnation point.

Acknowledgement: The authors thank Mr. S. Takenaka, Drs. T. Kinjo and S. Hyodo for their collaboration. This work was partly supported financially by the Core Research for Evolutional Science and Technology (CREST) of Japan Science Technology (JST) Agency (No. 228205R) and the Japan Society for the Promotion of Science through a Grant-in-Aid for Scientific Research (B) (No. 18360050).

References

Ansumali, S.; Karlin, I. V. (2002): Kinetic boundary conditions in the lattice Boltzmann method. *Phys. Rev. E*, vol.66, 026311.

Beskok, A.; Karniadakis, G.E. (1999): A model for flows in channels, pipes and ducts at micro- and nano-scales. *Nanoscale Microscale Thermophys. Eng.*, vol.3, pp.43-77.

Bhatnagar, P.L.; Gross, E.P.; Krook, M. (1954): A model for collision processes in gases. Small amplitude processes in charged and neutral one-component systems. *Phys. Rev.*, vol.94, pp. 511-525.

Cercignani, C. (1975): *Theory and Application of the Boltzmann Equation,* Scottish Academic Press.

Chapman, S.; Cowling, T.G. (1970): *The Mathematical Theory of Non-Uniform Gases,* Cambridge University Press, Cambridge, England.

Chen, C. K.; Chang, S. C.; Sun, S. Y. (2007): Lattice Boltzmann method simulation of channel flow with square pillars inside by the field synergy principle. *CMES: Comput. Model. Eng. Sci.*, vol. 22, pp. 203-215.

d'Humieres, D.; Ginzburg, I.; Krafczyk, M.; Lallemand, P.; Luo, L.-S. (2002): Multiple-relaxation-time lattice Boltzmann models in three dimensions. *Philos. Trans. R. Soc. London, Ser. A* , vol.360, pp.437-451.

Ginzbourg, I; Adler, P.M. (1994): Boundary flow condition analysis for the three-dimensional lattice Boltzmann model. *J. Phys. II France*, vol.4, pp.191-214.

Guo, Z.-L.; Zhao, T.-S.; Shi, Y. (2006): Physical symmetry, spatial accuracy, and relaxation time of the lattice Boltzmann equation for micro gas flows. *J. Appl Phys*., vol.99, 074903.

Guo, Z.-L.; Zheng, C.-G. (2009): Lattice Boltzmann methos for micro-scale flows. *Proc. 2nd Asian Symp. Comput. Heat Transf. Fluid Flow*, Jeju, Korea, Paper No. ASCHT09-K11.

Guo, Z.; Zheng, C.; Shi, B. (2008): Lattice Boltzmann equation with multiple effective relaxation times for gaseous microscale flow. *Phys. Rev. E*, vol.77, 036707.

Haile, J. (1997): *Molecular Dynamics Simulation: Elementary Methods*. John Wiley & Sons Inc.

Han, K.; Feng, Y. T.; Owen, D. R. J. (2007): Numerical simulations of irregular particle transport in turbulent flows using coupled LBM-DEM. *CMES: Comput. Model. Eng. Sci.*, vol. 18, pp. 87-100.

Hao, L.; Cheng, P. (2010): Lattice Boltzmann simulations of water transport in gas diffusion layer of a polymer electrolyte membrane fuel cell. *J. Power Sources*, vol. 195, pp.3870-3881.

Ho, C.-F.; Chang, C.; Lin, K.-H.; Lin, C.-A. (2009): Consistent boundary conditions for 2D and 3D lattice Boltzmann simulations. *CMES: Comput. Model. Eng. Sci.*, vol. 44, pp. 137-155.

Higuera, F. J.; Jimenez, J. (1989): Boltzmann Approach to Lattice Gas Simulations. *Europhys. Lett.*, vol.9, pp.663-668.

Karniadakis, G.; Beskok, A.; Aluru, N. R. (2005): *Microflows and Nanoflows: Fundamentals and Simulation*, Springer.

Keehm, Y.; Mukerji, T.; Nur, A. (2004): Permeability prediction from thin sections: 3D reconstruction and lattice-Boltzmann flow simulation. *Geophys. Res. Lett.*, 31, L04606.

Koplik, J.; Banavar, J.R. (1995): Continuum deductions from molecular hydrodynamics. *Ann. Rev. Fluid Mech*., vol.27, pp.257-292.

Lallemand, P.; Luo, L.-S. (2000): Theory of the lattice Boltzmann method: Dispersion, dissipation, isotropy,Galilean invariance, and stability. *Phys. Rev. E*, vol.61, pp.6546-6562.

Liou, W.W.; Fang, Y.C. (2000): : Implicit boundary conditions for direct simulation Monte Carlo method in MEMS flow predictions. *CMES: Comput. Model. Eng. Sci.*, vol.1 pp.119-128.

McNamara, G. R.; Zanetti, G. (1988): Use of the Boltzmann equation to simulate lattice-gas automata. *Phys. Rev. Lett.* vol. 61, pp. 2332-2335.

Nie, X.; Doolen, G. D.; Chen, S. (2002): Lattice-Boltzmann simulations of fluid flows in MEMS. *J. Statistical Phys.*, vol.107, pp.279-289.

Niu, X.-D.; Hyodo, S.; Munekata, T.; Suga, K. (2007): Kinetic lattice Boltzmann method for microscale gas flows: Issues on boundary condition, relaxation time, and regularization. *Phys. Rev. E*, vol.76, 036711.

Niu, X.-D.; Hyodo, S.; Suga, K.; Yamaguchi, H. (2009): Lattice Boltzmann simulation of gas flow over micro-scale airfoils. *Comput. Fluids*, vol.38, pp.1675-1681.

Niu, X.-D.; T. Munekata, T.; Hyodo, S.; Suga, K. (2007): An investigation of water-gas transport processes in the gas-diffusion-layer of a PEM fuel cell by a multiphase multiple-relaxation-time lattice Boltzmann model. *J. Power Sources*, vol.172, pp.542-552.

Ohwada, T.; Sone, Y.; Aoki, K. (1989): Numerical analysis of the shear and thermal creep flows of a rarefied gas over a plane wall on the basis of the linearized Boltzmann equation for hard-sphere molecules. *Phys. Fluids A*, vol.1,pp.1588-1599.

Pan, C.; Luo, L.-S.; Miller, C.T. (2006): An evaluation of lattice. Boltzmann schemes for porous medium flow simulation. *Comput. Fluids*, 35, pp. 957–965.

Peng, Y.; Luo, L.-S. (2008): A comparative study of immersed-boundary and interpolated bounce-back methods in LBE. *Progr. Comput. Fluid Dyn.*, vol.8, pp.156-167.

Sbragaglia, M.; Succi, S. (2005): Analytical calculation of slip flow in lattice Boltzmann models with kinetic boundary conditions. *Phys. Fluids*, vol.17, 093602.

Shen, C.; Tian, D. B.; Xie, C.; Fan, J. (2004): Examination of the LBM in simulation of microchannel flow in transitional regime. *Microscale Thermophys. Eng.*, vol.8, pp.423-432.

Stops, D. W. (1970): The mean free path of gas molecules in the transition regime. *J. Phys. D*, 3, pp.685-696.

Succi, S. (2002): Mesoscopic modeling of slop motion at fluid-solid interfaces with heterogeneous catalysis. *Phys. Rev. Lett.*, vol.89, 064502.

Suga, K.; Nishio, Y. (2009): Three dimensional microscopic flow simulation across the interface of a porous wall and clear fluid by the lattice Boltzmann method. *The*

Open Transp. Phenom. J., vol. 1, pp.35-44.

Suga, K.; Takenaka, S.; Ito, T.; Kaneda, M. (2010): Lattice Boltzmann flow simulation in a combined nanochannel. *Adv. Appl. Math. Mech.*, vol.2, pp.609-625.

Suga, K.; Takenaka, S.; Ito, T.; Kaneda, M.; Kinjo, T.; Hyodo, S. (2010): Evaluation of a lattice Boltzmann method in a complex nanoflow. *Phys. Rev. E*, vol.82, 016701.

Suga, K.; Tanaka, T.; Nishio, Y.; Murata, M. (2009): A boundary reconstruction scheme for lattice Boltzmann flow simulation in porous media. *Prog. Compt. Fluid Dyn.*, vol. 9, pp.201-207.

Toschi, F.; Succi, S. (2005): Lattice Boltzmann method at finite Knudsen numbers. *Europhys. Lett.*, vol.69, pp.549-555.

Verhaeghe, F.; Luo, L.-S.; Blanpain, B. (2009): Lattice Boltzmann modeling of microchannel flow in slip flow regime. *J. Comput. Phys.*, vol.228, pp.147-157.

Yu, H.; Luo, L.-S.; Girimaji, S. S. (2006): LES of turbulent square jet flow using an MRT lattice Boltzmann model. *Comput. Fluids*, 35, pp.898-909.

Zhang, Y.-H.; Gu, X.-J.; Barber, R.W.; Emerson, D.R. (2006): Capturing Knudsen layer phenomena using a lattice Boltzmann method. *Phys. Rev. E*, vol.74, 046704.

Zhang, Y.-H.; Qin, R.; Emerson, D.R. (2005): Lattice Boltzmann simulation of rarefied gas flows in microchannels. *Phys. Rev. E*, vol.71, 047702.

Zhang, R.; Shang, X.; Chen, H. (2006): Efficient kinetic method for fluid simulation beyond the Navier-Stokes equation. *Phys. Rev. E*, vol.74, 046703.